DISCLAIMER

This report was prepared as an account of work sponsored by an agency of the United States Government. Neither the United States Government nor any agency thereof, nor any of their employees, makes any warranty, express or implied, or assumes any legal liability or responsibility for the accuracy, completeness, or usefulness of any information, apparatus, product, or process disclosed, or represents that its use would not infringe privately owned rights. Reference herein to any specific commercial product, process, or service by trade name, trademark, manufacturer, or otherwise does not necessarily constitute or imply its endorsement, recommendation, or favoring by the United States Government or any agency thereof. The views and opinions of authors expressed herein do not necessarily state or reflect those of the United States Government or any agency thereof. Reference herein to any social initiative (including but not limited to Diversity, Equity, and Inclusion (DEI); Community Benefits Plans (CBP); Justice 40; etc.) is made by the Author independent of any current requirement by the United States Government and does not constitute or imply endorsement, recommendation, or support by the United States Government or any agency thereof.

Final Scientific/Technical Report

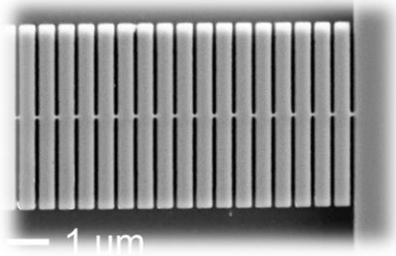

Award:	DE-AR0001056
Sponsoring Agency:	USDOE, Advanced Research Project Agency – Energy (ARPA-E)
Lead Recipient:	University of Colorado Boulder
Project Team Members:	Mahmoud I. Hussein, Kris A. Bertness, Ivan I. Smalyukh, Y.C. Lee (retired), Howard Branz (consultant)
Project Title:	Nanomanufacturing of Nanophononic Devices: Ultra-high ZT Thermoelectrics for Efficient Conversion of Waste Heat
Program Director	Dr. Laurent Pilon (January 2023 – June 2023) Dr. Joseph King (April 2019 – December 2022)
Principal Investigator:	Prof. Mahmoud I. Hussein (mih@colorado.edu)
Contract Administrator:	Laura Clayton (laura.clayton@colorado.edu)
Date of Report:	August 29, 2024
Reporting Period:	April 2, 2019 – June 30, 2023

This Report contains no Protected Data.

Public Executive Summary

Fabrication and Characterization Summary: For this program, the team fabricated and tested silicon thermoelectric test structures that experimentally demonstrated record thermal conductivity reduction (> 85 %) without changes in electrical properties (conductivity and Seebeck coefficient). We also demonstrated the highest ever reported energy conversion efficiency for silicon thermoelectric devices. The team developed a design for 1 cm^2 die with thousands of nanophononic metamaterial structures in the form of nanowalled membranes but were unable to solve all fabrication challenges before the end of the program. Multiple aspects of the design were submitted for patent protection. Primary challenges were related to silicon-on-insulator material quality and high-aspect-ratio etching.

Aerogels integration Summar: The team developed a process for manufacturing of lightweight superinsulation aerogel materials with compatibility with respect to other device development procedures and with mechanical robustness across a wide range of temperatures (sub-ambient to over 300C). Overall, these materials are fully adequate for the envisaged applications and can be manufactured with the help of solvent drying at conditions close to ambient conditions, thus making the manufacturing process cost-effective. The compatibility was tested and vividly demonstrated through various forms of imaging at scales from tens of nanometers to the device prototype scales (inches).

Assembly and Device Level Characterization Summary: The team developed methods to assemble 1 cm^2 die with metal bus bars in stacks layers and supported by copper blocks. The assembly included pick-and-place equipment to align die, silver nanoparticle adhesion layers, and openings for introduction of aerogel. The team also developed a vacuum fixture using a mini oven design for measuring the thermal conductivity, heat flow, and electrical power generation in such a completed device. This fixture was tested with conventional thermoelectric devices and known materials and found to be accurate with a few percent.

Theory and Simulations Summary: The team conducted an extensive computational investigation of the proposed nanophononic metamaterial configurations utilizing advanced techniques including lattice dynamics and molecular dynamics simulations. The nanoscale effects of size (and upscaling), disorder, doping, and surface roughness on the thermal conductivity of the nanophononic materials were thoroughly investigated. These studies established that (1) thermoelectric performance can be preserved, and in some aspects, improved with moderate increases in size, (2) disorder in the nanoresonator locations can bring rise to Anderson localization and cause further reduction in the thermal conductivity, and (3) moderate levels of doping and surface roughness are permitted. The theory and simulations also further developed the criteria for optimal geometric design of the nanopillared or nanowalled membranes.

Acknowledgements

The PI and co-PI team acknowledge ARPA-E for its funding and support of this research, and are grateful to Drs. Joseph King (April 2019 – December 2022) and Dr. Laurent Pilon (January 2023 – June 2023) for directing the program, and Dr. Ashok Gidwani for this role in assisting the program directors and supporting the team. The team are also grateful to Dr. Howard Branz for this advisory role throughout the research, Dr. Y.C. Lee for his contributions to the project prior to his retirement, Prof. Eric Toberer for his contributions during the earlier parts of the research, and all the postdocs, PhD, MS, and BS students who worked diligently on the research. The team is also thankful to the University of Colorado Boulder for offering its facilities and resources during the regular team and review meetings throughout the project.

Table of Contents

Table of Figures/Tasks

Accomplishments and Objectives

Fabrication and Characterization Accomplishments: The team met its initial objectives of demonstrating a thermal conductivity reduction in test structures and in microscale thermoelectric generators. Although the team achieved record reductions in thermal conductivity and thermoelectric power generation in a silicon-based device, they did not achieve the quantitative objectives for the program. Major accomplishments in this area are:

- Record thermal conductivity reduction of > 85 % in multiple test structures with no degradation of electrical properties
- Record thermoelectric power conversion efficiency in a silicon-based device of 0.19%
- Novel etch mask and design integration methods developed and submitted for patent protection

Aerogels Accomplishments: All aerogel-related objectives were accomplished, albeit some with a somewhat delayed timeline due to impacts of the pandemic. In particular, thermal conductivity values significantly lower than that of still air could be achieved in a mechanically robust aerogel material, well below the target of 12mW/(Km) across a wide range of subambient/ambient/elevated temperatures. Importantly, our extensive characterization of mechanical, thermal, and other properties revealed that our aerogel materials are suitable for both nanoscale and device-scale integration with nanophononic thermoelectric structures. A manuscript is being prepared, in addition to this report, to document our accomplishments in this area.

Assembly and Device Level Characterization Accomplishments: The team met its objectives in preparing assembly and TE device-level characterization fixtures; however, they were unable to meet the objective of fabricating a large-area silicon nanophononic metamaterial device by the end of the program. Major accomplishments in this area are:

- Developed a packaging approach including aerogel incorporation and nanoparticle silver adhesion layers for connecting multiple silicon thermoelectric elements
- Fabricated and tested a vacuum fixture based on a mini oven approach to test 1 cm^2 die of assembled silicon thermoelectric elements

Theory and Simulations Accomplishments: The team was successful in meeting its objective of the creation and analysis of a wide range of complex atomic-scale models of nanopillared and nanowalled membranes incorporating foreign chemical elements substituted into silicon to represent doping and/or surfaces with atomic-scale surface topologies spanning a wide range of statistical parameters to represent real nanoscale surfaces. The team was also able execute large-scale high-capacity computing to model the size effects and determine the optimal criteria for upscaling the nanophononic material structures while improving the performance as measured by the degree of thermal conductivity reduction. Furthermore, the research utilized advanced models of spectral energy analysis to characterize the improvement of performance with moderate levels of disorder. Each of these contributions have fed valuable knowledge into the experimental part of the program.

Project Activities

1. Fabrication and Characterization Summary (Senior Personnel Bertness):

For this program, we fabricated and tested silicon thermoelectric test structures that experimentally demonstrated record thermal conductivity reduction (> 85 %) without changes in electrical properties (conductivity and Seebeck coefficient). We also demonstrated the highest ever reported energy conversion efficiency for silicon thermoelectric devices. Primary challenges were related to silicon-on-insulator material quality and high-aspect-ratio etching.

Thermal Conductivity Reduction

A major accomplishment of this program was the demonstration of large reductions in thermal conductivity due to the nanophononic metamaterial (NPM) effect. The test structures used for this part of the program and their dimensional definitions are illustrated in Fig. 1. The membrane is formed by etching from the top down resulting in a membrane that is perpendicular to the substrate surface. NPM membranes also have many walls extending perpendicular to the membrane plane on both sides. The premise of the NPM effect is that the stationary phonon modes in the walls will couple with the phonon modes in the membrane and slow heat transport. Increasing wall height increases the number of stationary phonon modes and thus is expected to produce greater reductions in thermal conductivity.

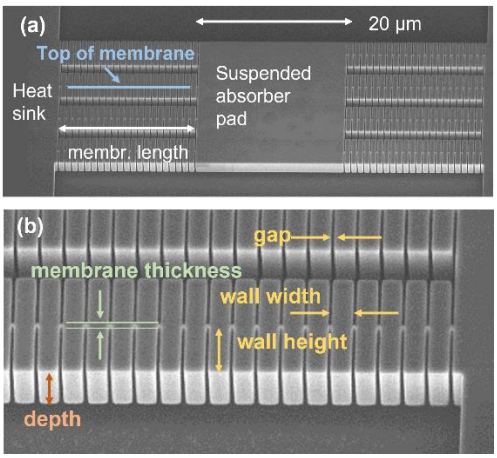

Figure 1. (a) Overview of structure. (b) Definition of dimensional parameters for membranes and NPM walls.

The key data from this effort is shown in Fig. 2(a) in which the reduction of the membrane thermal conductivity with wall height is shown for three different patterns that have the minimum membrane thickness achieved in this set, about 90 - 110 nm, and varying wall widths. The thermal conductivity calculation includes determining an effective thermal cross-section for the heat flow based on Fourier diffusive models of heat transport. This transport model is not likely accurate for very small structures, however, and we can extrapolate the correction to the cross-section by with a theoretically calculated "beta factor." This correction indicates that classical transport theory underestimates the thermal cross-section, and, when corrected, the effective cross-section for phonon transport is larger than the classical cross-section and therefore the actual thermal conductivity becomes smaller. This beta correction ranges from zero for unwalled membranes to 1.63 for membranes with tall walls. The beta-corrected points for pattern c5 are shown as purple triangles. Similar changes would be calculated for the c11 and c8 data but are omitted from the graph for clarity. The lowest values of thermal conductivity, around 3.8 ± 0.3 W/m·K, are lower than any other experimental data for silicon membranes [1], with 7.4 W/m·K being the lowest reported for a 7 nm thick membrane [2]. This achievement is all the more remarkable because the membrane thickness in our experiment was >10x greater than its nearest competitor.

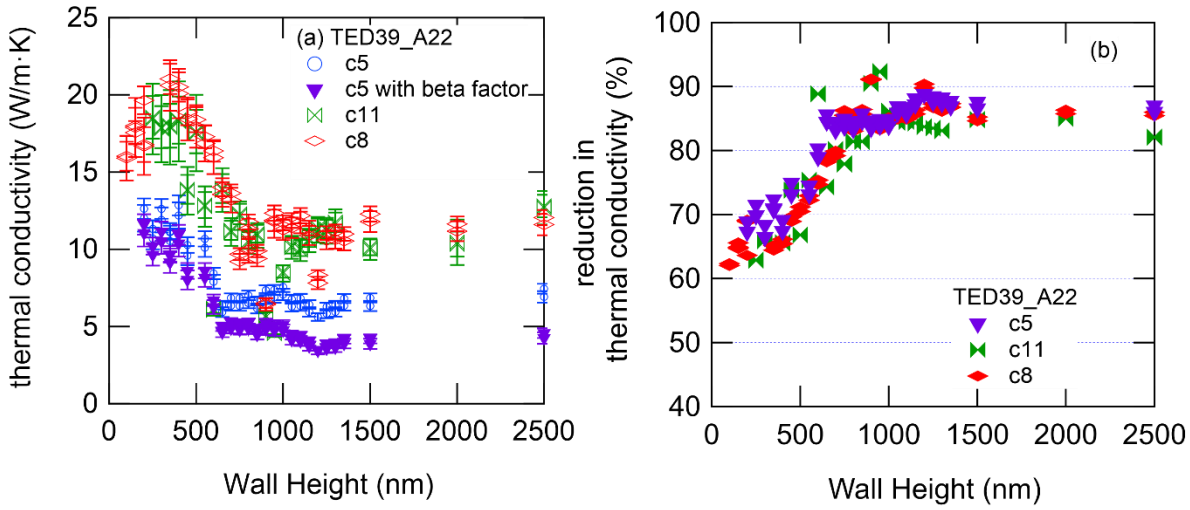

Figure 2. Thermal conductivity reduction in NPM membranes as a function of wall height for membrane sets with different wall widths (c5: 240 nm, c8: 640 nm, c11: 445 nm). (a) Thermal conductivity values, and (b) percent reduction relative to unwalled membranes with the same equivalent membrane thickness. Solid symbols include the beta factor correction.

The percentage reduction in thermal conductivity for the same data set is shown in Fig. 2(b). We achieved thermal conductivity reductions of >= 85 % for over twenty samples. The reduction in thermal conductivity for thin silicon membranes relative to bulk silicon is well-established the scientific literature, so to isolate the NPM reduction from the thin-membrane reduction, we fabricated and characterized unwalled membranes in nearby regions of the same substrate. These data were modeled with a smooth curve and interpolated to find the thermal conductivity of an unwalled membrane with the same equivalent membrane thickness (the effective cross-section divided by the depth) as the NPM membrane. We note that the reduction in thermal conductivity calculated from the "bulk" SOI value is 95% for the structures with the lowest thermal conductivities. This data satisfies one component of Milestone 2.2.

Independent Mechanism for Thermal Conductivity Reduction

A major advantage of our approach for thermal conductivity is that the nanowalls, in principle, do not impede current flow or change the Seebeck coefficient of the membrane, unlike approaches that add scattering centers in the path of heat and current flow. As part of this project, we demonstrated that this advantage applies in practice as well. Comparisons between NPM (walled) and unwalled membranes showed that there is no statistically significant difference between two the types for conductivity or Seebeck coefficient. For measuring the Seebeck coefficient (and power conversion efficiency), the suspended structure was modified to contain NPM (or unwalled) membranes on the left side, and a long leg that electrically shorts the absorber pad to ground and allows us to measure the Seebeck voltage generated across the membranes. We also showed that aerogel integration in the test structures did not affect these measurements, meeting the requirements of Milestone 2.2.

Record Energy Conversion Efficiency for a Silicon Device

To make a full evaluation of the energy conversion efficiency for our NPM structures, we developed the microgenerator device as a variation of the asymmetric device developed for Seebeck coefficient measurements. The electrical contact pads were wire-bonded to a small piece of printed circuit board with pins that allowed electrical connection of the hot and cold membrane sides to an external variable load resistor via a vacuum feedthrough. The electrical power generated in the load resistor was measured and compared with the thermal power input to measure the energy conversion efficiency. We achieved a

maximum efficiency of 0.19 % for $\Delta T = 390$ K. Based on a comprehensive literature search, this value is a world record for a "black box" efficiency measurement of a silicon thermoelectric device, that is, through direct measurement of both electrical and thermal power. The two other reported values are 0.007 % [3] and 0.0006% [4]. In fact, most papers on the topic of silicon thermoelectrics do not report an efficiency measurement, but rather report measurements of the materials properties that factor into the figure of merit *ZT*, specifically electrical conductivity σ, thermal conductivity κ, and Seebeck coefficient or thermopower *S*, and then extrapolate to efficiency based on analytical equations assuming ideal fabrication and testing conditions. We are able to measure a true power conversion efficiency because our structures are large (> 1 μm) in most dimensions, and even our smallest dimension, the membrane thickness at around 100 nm, is significantly larger than silicon nanowire devices with diameters of 10 nm to 20 nm.

Challenges and Future Outlook

We have conclusively demonstrated the NPM effect and set records for thermal conductivity reduction and energy conversion efficiency in silicon-based thermoelectric devices. Nevertheless, we fell short of our ambitious milestone goals for this program, 8 % efficiency in Milestone 2.3 and 18 % efficiency for a prototype device in Milestone 3.2. One challenge appears to be the unexpectedly low and variable thermal conductivity of our starting material, SOI device layers. We were unable to identify the nature of the defects that reduced phonon transport, which in turn would be expected to reduce the resonant coupling that leads to the NPM effect and therefore reduce the NPM effect. Late in the program, we obtained two epitaxial silicon substrates on higher quality SOI and found that these substrates displayed higher thermal conductivity. There was insufficient time left in the program to fully test this material. We also observed that the geometrical guidelines arising from the nanoscale theoretical simulations did not fully carry over into the larger experimental test structures. Further thermoelectric efficiency improvements are likely possible by a broader range of geometrical variations in test structures on these substrates. In short, we have not yet reached any fundamental physical limits to further progress and anticipate significant progress with additional work.

2. Aerogels Research (Co-PI Prof. Smalyukh)

A key aspect of the research program was the investigation of aerogel as supporting materials for the target silicon/NPM-based device, with the aim of serving two functions: (1) structural support of the NPM structural components within the overall device configuration and (2) decreasing the internal thermal lost due to thermal conduction. For the practical application of an aerogel in our target devices, it was also critical to investigate the compatibility of the aerogel as fabricated with the NPM structure especially considering the nanoscale nanopillar features.

After development and polishing of the aerogel chemical synthesis and fabrication process, the next key part of the investigation focused on characterization of the aerogel's mechanical properties with different air porosities and at different temperatures. Silica aerogel with densities 0.08 g/cm3 (94% porosity), 0.136 g/cm3 (91% porosity), and 0.2 g/cm3 (88% porosity) were synthesized and the effects of temperature on the compression and tensile mechanical properties were studied. The temperatures studied are 20$_o$C, 100^{o}C, 200^{o}C and 300^{o}C for compression and in tensile pulling analysis. Fig. 3(a) shows the compression stress-strain curves of the least porous (88%) aerogel samples at different temperatures. In the samples investigated, the elastic modulus *E* was found to vary from 1.7 MPa to 2.5 MPa, a substantial increment (47%) with temperature on a compressive strength of 0.8 MPa and a fracture strain from 33% to >45%. The sample under room temperature has given the stress-strain curve with the largest ultimate strain (45%) before it

fractured. The sample at highest temperature (300°C) shows the highest modulus behavior however the sample was more brittle and less ductile. A similar trend is observed with the high porosity (91%) aerogel where the elastic modulus *E* of the sample was found to vary from 1.25 MPa to 1.8 MPa, with an increment of 44% at high temperature (Fig. 3(b)). The compressive strength of the sample was 0.75 MPa and a fracture strain from 40% to 57%. The most porous sample we studied (Fig. 3(c)) has shown the best compressive fracture strain ranging from 60% to 75%. The elastic modulus *E* of these samples were found to vary from 1.15 MPa to 1.4 MPa, with an increment of 20% at highest studied temperature. The detailed analysis shows that the failure modes of the aerogels were observed to be highly density- and temperature- dependent.

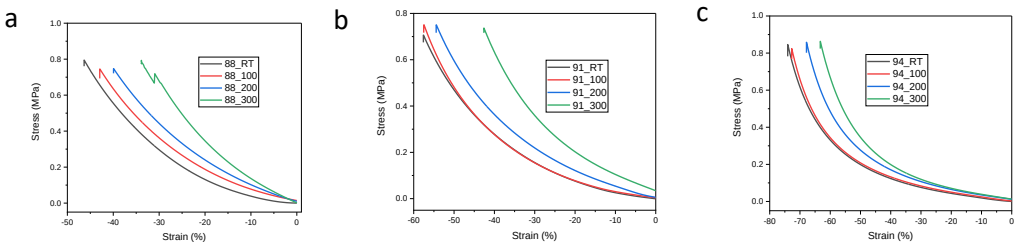

Figure 3. Stress–strain curves measured under compression loads with aerogels under varying temperatures and porosity 88% (a), 91% (b) and 94% (c).

Another critical property that we characterized was the thermal conductivity of the aerogel, as well as testing of performance at relatively conditions of a temperature difference reaching 300C. The measurement results are shown in Fig. 4. We observed a thermal conductivity reaching below the 12mW/(K.m) milestone target.

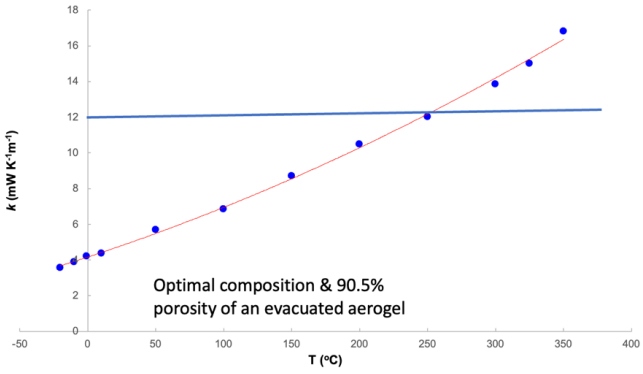

Figure 4. Experimental characterization of thermal conductivity for a vacuum-packaged aerogel with optimal composition and morphology defined by CTAB-templating and porosity of 90.5%.

The other key aspect that the aerogel team focused on is ensure adequate integration of aerogels within the NPM nanostructures. We successfully demonstrated the aerogel encapsulation processes for device assemblies on a sapphire carrier by following an established procedure. Fig. 5 shows Si test chips bonded on top of sapphire carrier and copper caps sintered on top of Si test chips. The wafer-bond remover successfully released the Si chips from the sapphire carrier without damaging aerogel encapsulation.

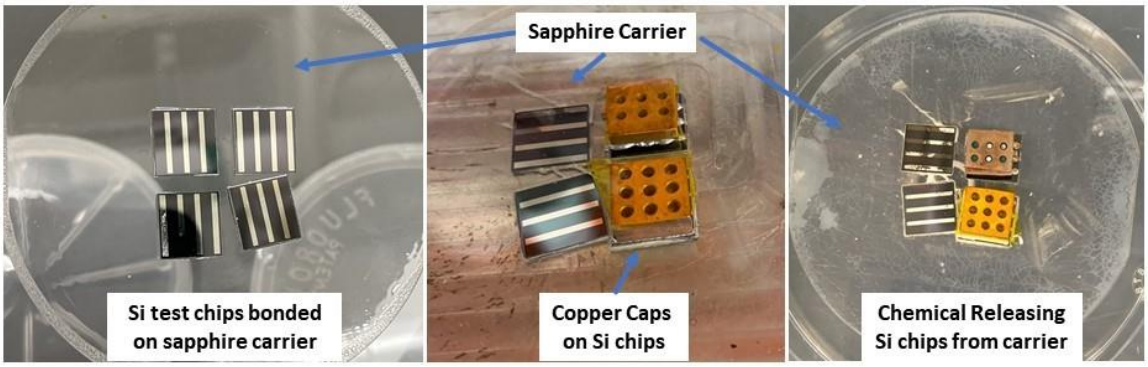

Figure 5. Example of the thermoelectric device assemblies bonded on top of a sapphire carrier with aerogel encapsulation.

Summary, Challenges, and Future Outlook

We have performed a wide range of mechanical characterizations at elevated temperatures and demonstrated control of the mechanical properties to avoid occasional cracking of aerogel during the final assembly via improving adhesion of aerogel to copper surfaces. A challenge that we faced, and resolved pertains to the compatibility of the process that resulted in oxidation in relation to integration of aerogels with metal structures. We have shown it being fully compatible with the aerogel drying and preparation procedures. The extensive mechanical characterization and integration studies reveal that our aerogels are suitable for thermal packaging of the NPM-based thermoelectric devices. Future work will focus on testing performance of the aerogels when subjected to large thermal gradients (>300C difference on hot/cold sides), and testing the performance in the final device realization.

3. Device Integration, Assembly and Test Fixture (PI Hussein, formally Co-PI Lee)

The device integration, characterization, and assembly team developed during the course of the program. The process developed for packaging of the NPM-based thermoelectric device uses sintered silver nanoparticles. The design comprises bonding copper caps to the NPM-based device to ensure a strong connection as well as high thermal and electrical contact between the copper caps and the chip. The team developed silicon chips for process development. Figure 6 depicts one of the copper caps and the chip used to develop the sintering process. As shown in the figure, there are three pads on the silicon chip which will be bonded to the fingers in the copper cap. The surface of the copper cap and the pads are coated with silver before bonding. For coating a 25 nm chromium layer is evaporated first and on the top of it, a 250 nm silver layer is evaporated. The chromium layer acts as an adhesion layer.

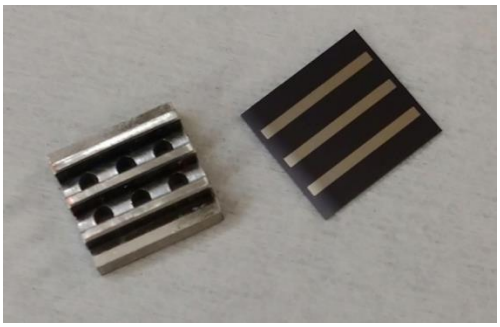

Figure 6. The silicon chip and the copper cap used to develop the packaging process.

Several challenges existed in bonding using sintered silver The first was aligning the fingers in the copper cap with the pads with a submillimeter resolution. If the alignment is bad, then some of the nanoparticles will penetrate the NPM-based device and cause damage. To address this problem, the team designed an alignment fixture intended to fix the location of the chip so that the copper cap can move vertically onto it while the fingers are aligned with the pads. We successfully addressed this issue. Figure 7 shows the alignment fixture design.

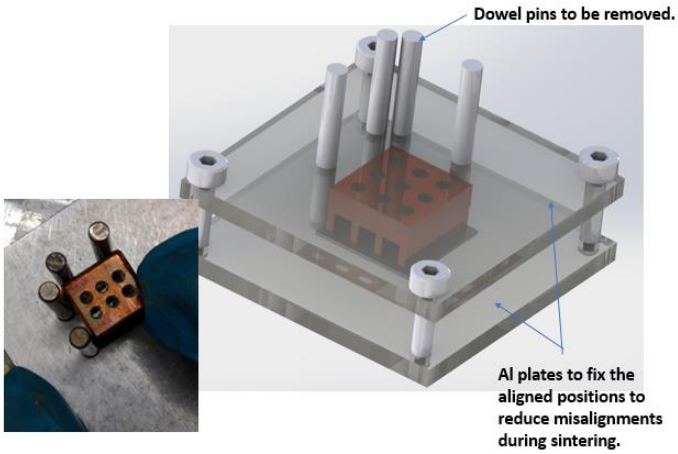

Figure 7. Alignment fixture for bonding an assembly and a revised fixture to be developed.

The second challenge is the spillover, which happens when excessive nanoparticles exists at the interface between the copper caps and the chips. Spillover can cause the nanoparticles to penetrate the NPM structures and potentially damage them. Other challenges are the bonding strength and bonding quality. To improve the spillover, the team created a chamfer at the fingers of the copper caps that was bonded to silicon pads. Figure 8 shows the method used to reduce spillover.

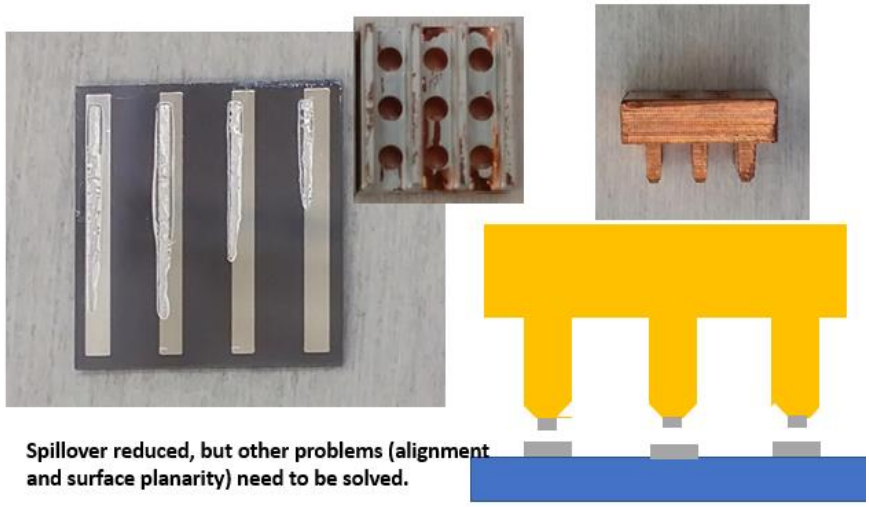

Figure 8. Chamfered copper fingers used to reduce spillover. The misalignment problem is to be fixed in the next quarter.

As for the characterization setup, the team took inspiration from a mini oven approach developed at MIT. The setup as shown in Fig. 9 has mini oven that is controlled using PID feedback loop to maintain similar temperature as that of the main heater that is housed inside the oven. This creates an isothermal environment

around the main heater. The PID feedback loop is implemented on LabVIEW using the feedback from the built-in thermocouples in the oven which compare against the setpoint values measured through a thermocouple in the main heater. The power to the heaters in the oven is controlled through a programmable DC power supply which receives commands from the PID loop. The design, furthermore, allowed for the reduction of the size of the main heater to reduce the surface area, thereby reducing the heat leakage. We ensured our mini oven encloses just the main heater and the hot side copper cap of the NPM-based device and made use of a vertical stage to press the sample between hot and cold sides making it demountable.

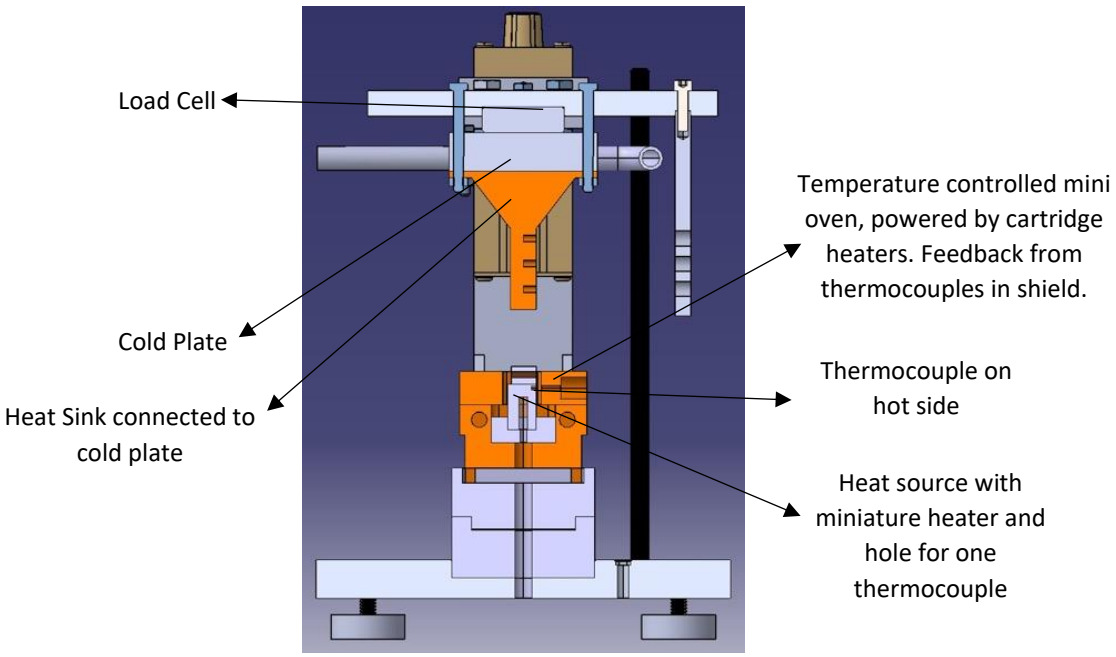

Figure 9. Schematic of the modified setup with mini oven and smaller main heater.

Through simulations, we found this approach to have a heat flow efficiency of 90-97%, depending on the thermal resistance of the sample, from the heater to through the sample. The process was tested yielding successful results.

Summary, Challenges, and Future Outlook

The team develop a robust device integration and assembly technique that uses sintered silver nanoparticles. The design comprises bonding copper caps to the NPM-based device to ensure a strong connection as well as high thermal and electrical contact between the copper caps and the chip. In future work, the team will apply the process to a actual NPM-based device once prepared. In addition, a robust thermoelectrical properties device-level characterization technique was developed based on a mini oven approach. The characterization set up was tested and well calibrated.

4. Theory and Simulations (PI Hussein)

The theory/simulations group has investigated a series of problems to evaluate the performance of NPMs under various design and “as-fabricated” conditions. This included investigating the effects of size, disorder, surface roughness, and doping.

Effect of size

From a practical point of view, NPMs are realizable in sizes substantially larger than the cases considered in our theoretical/computational studies. This is owing to feasibility considerations for nanofabrication [5] and efficient device integration [6]. With the continued development of high-capacity computing, NPM unit cells of larger sizes will be investigated in the future. In the course of this program, however, it was beneficial to examine the relative trends in performance for various computationally tractable NPM configurations (and a corresponding NPC for comparison) as the overall size increases. In particular we have studied the effect of proportionally increasing the unit-cell size specifically along the planar directions.

We consider the following nanostructures are depicted in Fig. 10 NPM_1, NPM_3, NPM_{60}, and NPC. We investigate varying the base membrane width b while keeping d constant and the ratio c/b fixed to 2/3. These variations in dimension keep the nanopillar-to-base-membrane volume faction fixed for each configuration to 0.67 for NPM_1, 1.34 for NPM_3, and 26.67 for NPM_{60}. The in-plane thermal conductivity was calculated for the cases listed in Table 1. For each case, we also report k_{NPX}/k_{Memb}. The results are plotted in Fig. 11.

Table 1: Choice of dimensions for thermal conductivity predictions plotted in Figure FT-2.

Configuration	b/a [CC]	c/a [CC]	d/a [CC]	h/a [CC]
Membrane	18	N/A	18	N/A
NPC	6,9,...,18	4,6,...,12	18	N/A
NPM_1	6,9,...,18	4,6,...,12	18	18
NPM_3	6,9,...,18	4,6,...,12	18	54
NPM_{60}	6,9,...,18	4,6,...,12	18	1080

It is observed that as the size of NPM_1 is proportionally increased in the lateral directions, the thermal conductivity ratio k_{NPX}/k_{Memb} drifts slightly upward. This trend is attributed to deterioration in the degree of vibron–phonon DOS conformity as the unit-cell size increases while keeping the volume fraction fixed. However, this deterioration is less significant for NPM unit cells with larger volume fractions. Indeed this is noticed in Fig. 11 when examining the slope of the rise of k_{NPX}/k_{Memb} for the various NPM configurations. NPM_3 experiences a milder rise compared to NPM_1, and NPM_{60} experiences no noticeable change as the lateral size of the unit cell is increased. As reported by Honarvar and Hussein [7], the slope of the k_{NPX}/k_{Memb} trend with size may be rendered negative when the volume of the nanopillar is increased at a higher rate as the volume of the base-membrane portion is increased. This phenomenon has been described as the "compensatory effect."

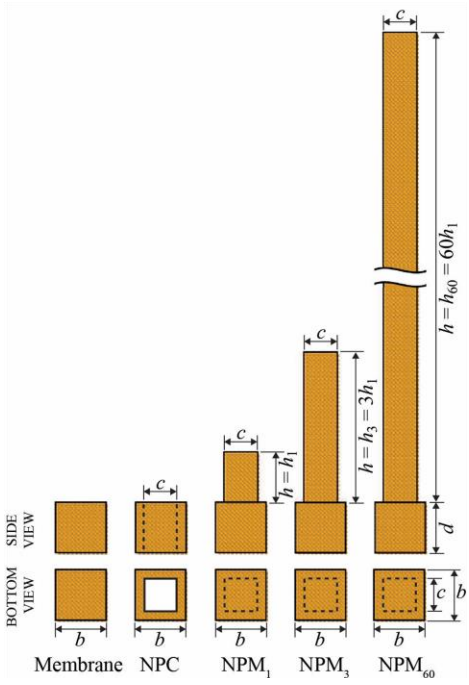

Figure 10. Schematics representing five membrane-based material systems considered in this investigation. NPM_1, NPM_3, and NPM_{60} are identical except for the nanopillar heights. The width of the nanoholes in NPC is identical to the width of the nanopillars. All membranes have identical base dimensions and thickness and are made out of Si.

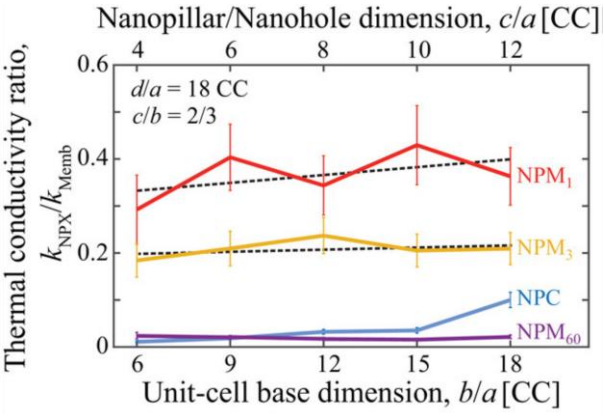

Figure 11. Effect of varying unit-cell base size: Thermal conductivity reduction versus separation distance between nanopillars for three membrane-based NPMs with different nanopillar heights but a fixed membrane thickness. A comparison is provided for a corresponding membrane-based NPC where the separation distance between the nanoholes is varied in the same way. Schematics of all four unit cells are given in Figure 3.2. All results are normalized with respect to the thermal conductivity of a uniform membrane with the same thickness. All results are for d = 9.78 nm and c/b = 2/3.

Effect of disorder

We investigated the effect of randomly disordered nanowall heights in NPMs (considering a volume fraction of 10). An NPM with a volume fraction of 1.1, and another with a volume fraction of 2.2 were considered. In both cases, the thermal conductivity was calculated–via MD simulations–as a function of the strength of disorder. The results have shown a 27% and 30% reduction in the thermal conductivity, respectively. In an additional study, we set up a new NPM model encompassing disordered nanowalled (rather than nanopillared) membranes with a volume fraction of 10, which is a significantly larger than the previous cases. This study yielded excellent results as shown in Fig. 12 and summarized as follows:

• With a large value of nanowall-to-membrane volume fraction, V_r=10, the thermal conductivity was shown to drop by ~75% due to disorder in the nanowall heights. This reduction is additional over the reduction by solely the NPM effect.
• Most of the thermal conductivity reduction takes place with a small level of disorder; with lesser and lesser impact as the intensity of disorder is increased.
• The error bars for the thermal conductivity predictions are much smaller for V_r=10 than those for smaller values of V_r. This shows that the more saturated the phonon band structure is with resonances, the lower the sensitivity to statistical variations in the model and simulations parameters.

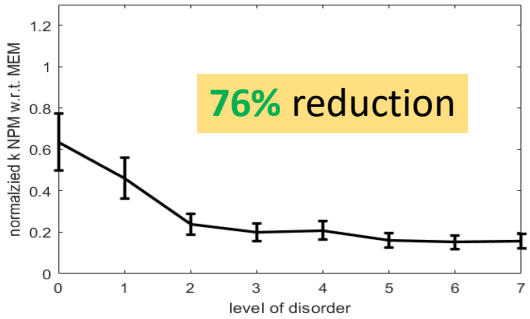

Figure 12. Seven configurations of all-silicon NPMs in the form of nanowalled membranes were considered, one with perfectly identical nanowall heights, and six with non-uniform nanowall heights with increasing level of statistically generated disorder. Each model consisted of a membrane with 30 nanowalls erected on one surface. The level of disorder is measured by the standard deviation from a normal distribution; this quantity is proportional to the parameter n_i plotted in the *x*-axis. The higher the n_i value, the higher the level of disorder. This system has an average volume fraction of V_r=10.

Effect of surface roughness

We have shown by MD simulations that an NPM with a nanopillar exhibiting pristine surfaces experience stronger drops in the thermal conductivity compared to a corresponding NPM with roughened nanopillars. This result provided an additional "proof" of the NPM effect since this behavior may only be possible if the effects of resonance exceed the effects of roughness. With this result, the Q6 milestone concerning the effect of roughness has been fulfilled. We first considered a uniform (unpillared) membrane and examined different cases with a gradual varying of the intensity of roughness. As expected, the thermal conductivity was shown to decrease with the level of roughness; see blue curve in Fig. 13. We then conducted the same investigation on the same membrane but with nanopillars added. Strikingly, the results show an increase, rather than a decrease, in the thermal conductivity as the roughness of the nanopillar surfaces is increased. This indicates that as the nanopillars become smoother the NPM effects increases and dominates the reduction in the thermal conductivity (i.e., outweighs the effect of boundary scattering from rough surfaces). Importantly, this result appears in a monotonic trend, which provides further profound evidence of the NPM effect. The NPM results are shown by the red curve in Fig. 13.

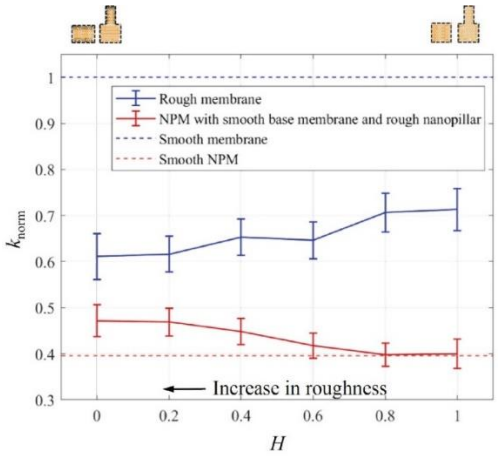

Figure 13. In-plane lattice thermal conductivity for a membrane and a corresponding nanopillared membrane (NPM) versus the Hurst factor *H*. As *H* decreases, the level of roughness increases. The blue curve depicts the membrane and the red curve the NPM. The clear opposite trends provides further evidence of the presence of the NPM effect.

Effect of doping

We conducted an MD investigation to study the effect of phosphorus-doping on the thermal conductivity of Si-based NPMs. Doping is necessary for achieving a relatively high power factor for an NPM. However, its concentration values need to be optimized because excessive doping could lead to undesired levels of additional scattering of the phonons which in turn would hinder the role of resonances in reducing the NPM thermal conductivity. A large set of simulations of NPMs were executed considering a range encompassing the NIST P-dopant concentrations, from 1.45×10^{17} to 5×10^{19}. Figure 14 shows the results obtained. It is observed that the thermal conductivity is reduced by over 35% due to the presence of doping at a concentration of 100.07×10^{18} cm^{-3}. It should be noted that a proper modeling of P-Si interactions has been utilized by adopting a potential suited for this problem (Liu et al. *Comput. Mater. Sci.*, 120, 1-12, 2016). The results show that the NPM performance is immune to doping up to a concentration of 5×10^{19}. This provided a valuable theory-based limit for the doping concentration for the NIST experiments.

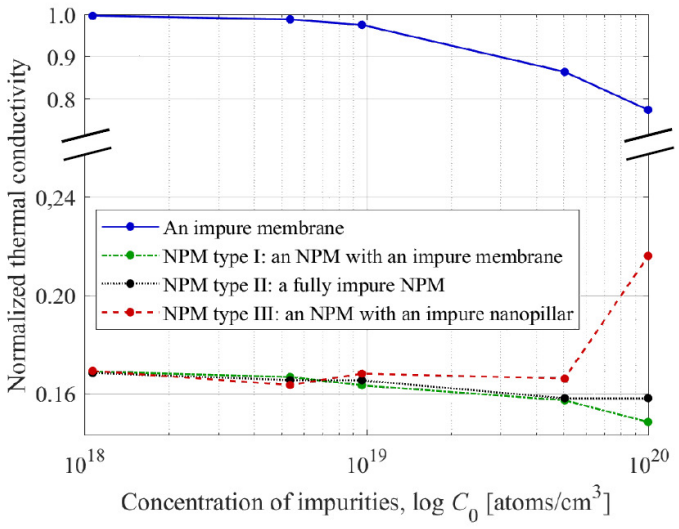

Figure 14. Thermal conductivity of NPM versus dopants concentration considering different regions in the NPM where the dopants are included. The choice of dopants is made to cover the range 1.08×10^{18} to 100.07×10^{18} cm^{-3}. This range encompasses the concentration values observed in the NIST samples.

Summary, Challenges, and Future Outlook

The theory/computational simulations have produced results pertaining to the effects of surface roughness that are directly relevant to experiments. A wide range of realistic models of surface roughness were generated yielding a conclusion that the nanopillars must be as smooth as possible to maximize the NPM effect. However, the results also show a level of robustness as the thermal conductivity reduction deterioration with roughness happens gradually with the increase in the roughness parameters. It was shown that an upper limit of dopant concentration of 5×10^{19} is allowed to improve electrical properties without affecting the NPM effect. This provides direct guidance to the design process for nanofabrication.

Regarding size effects, the models analyzed were overly small compared to experimental dimensions due to computational constraints. However the results have validated the trends predicted by theory, confirming that the nanopillar-to-base-membrane volume fraction must be as large as possible (within the allowable phonon mean free path range at the temperature of interest) in order to maximize the NPM effect.

Finally, the disorder study—while also done at very small computational model sizes compared to experiments—demonstrated that a significant additional reduction in the thermal conductivity is possible, primarily due the added effect of Anderson localization.

Future work would seek to extend the sizes of the computational models further to reach the lower limit of experimental scales. Only then, we would be able to have a direct assessment of the size effects for silicon-based NPMs. Such models would also need to incorporate some impurities/doping and surface roughness, following the modeling schemes we developed in the program in order to provide a more accurate prediction of the behavior of as-fabricated experimental NPM samples.

References:

[1] B. Fu, K.D. Parrish, H.-Y. Kim, G. Tang and A.J.H. McGaughey, "Phonon confinement and transport in ultrathin films," *Phys. Rev. B*, **101** (4), (2020), DOI: 10.1103/PhysRevB.101.045417.

[2] S. Neogi, J.S. Reparaz, L.F.C. Pereira, B. Graczykowski, M.R. Wagner, M. Sledzinska, A. Shchepetov, M. Prunnila, J. Ahopelto, C.M. Sotomayor-Torres, and D. Donadio, "Tuning Thermal Transport in Ultrathin Silicon Membranes by Surface Nanoscale Engineering," *ACS Nano*, **4** (9), 3820, (2015).

[3] G. Hu, H. Edwards and M. Lee, "Silicon integrated circuit thermoelectric generators with a high specific power generation capacity," *Nature Electronics*, **2** (7), 300, (2019), DOI: 10.1038/s41928-019-0271-9.

[4] K. Ziouche, Z. Yuan, P. Lejeune, T. Lasri, D. Leclercq and Z. Bougrioua, "Silicon-Based Monolithic Planar Micro Thermoelectric Generator Using Bonding Technology," *J. Microelectromech. Sys.*, **26** (1), 45, (2017), DOI: 10.1109/jmems.2016.2633442.

[5] Abhijit Biswas, Ilker S Bayer, Alexandru S Biris, Tao Wang, Enkeleda Dervishi, and Franz Faupel, "Advances in top–down and bottom–up surface nanofabrication: Techniques, applications & future prospects," *Advances in Colloid and Interface Ccience*, **170**(1-2):2–27, 2012.

[6] Boon K Teo and Xu Hui Sun, "Silicon-based low-dimensional nanomaterials and nanodevices," *Chemical Reviews*, **107**(5):1454–1532, 2007.

[7] Hossein Honarvar and Mahmoud I Hussein, "Two orders of magnitude reduction in silicon membrane thermal conductivity by resonance hybridizations," *Physical Review B*, **97**(19):195413, 2018.

Milestones

Tasks	Milestones and Deliverables
Task 1: **Project Direction and Theory to Mitiigate Risks**	
M1.1 Go/No-Go: Refine tasks and milestone	**Baseline End: 07/01/19 (Q1)** **% Comp 100%** Description: Modeling that extends the nanophononic theory to provide predictions within the range of nanodimensions that be experimentally fabricated Performer Summary: Completed during first review meeting on July 29, 2019.
M1.2 Model upscaling	**Baseline End: 04/01/20 (Q4)** **% Comp 100%** Description: Modeling that extends the nanophononic theory to provide predictions within the range of nanodimensions that be experimentally fabricated Performer Summary: Impact of COVID-19 has slowed down the CU Theory/Simulations team which lead to a delay in completion of the large-scale size effects studies. During Q6, the team established completion of the large-scale NPM size effects investigation, and hence fulfillment of the M1.2 milestone. Please see submitted Q6 report for more details.
M1.3 Theory: Roughness and interface effects	**Baseline End: 10/01/20 (Q6)** **% Comp 100%** Description: Theory predictions of roughness and interface tolerances for high ZT. Performer Summary: Impact of COVID-19 has created exceedingly long queue times in

	the Argonne supercomputer for the CU Theory/Simulations team which lead to a delay in completion of the roughness effects studies. However, during Q7, the team completed this investigation and fulfilled the M1.3 milestone.
M1.4 Go/No-Go: Theory: NPM performance improvement strategies	**Baseline End: 10/30/21 (Q10)** **% Comp 100%** Description: Theory predictions for adding alloying in base membrane and disorder in nanowalls to maximize ZT performance. Performer Summary: Our investigation on disordered NPMs was completed during Q1-Q5 and our investigation on the effects of doping on NPM performance was completed during Q3-Q5. As shown in Fig. Q5-12 (from the Q5 report), it was demonstrated that an additional reduction of up to 75% in the NPM in-plane thermal conductivity can be achieved by disordering the nanowalls on top of the reduction due to the NPM effect. And as shown in Fig. Q5-13 (also from the Q5 report), it was demonstrated that an additional reduction of up to 35% in the NPM in-plane thermal conductivity can be achieve by adding phosphorous doping on top of the reduction due to the NPM effect—as long as the dopants are limited to the base membrane portion. These results demonstrate the disordering and the addition of dopents (when done only in the base membrane portion of the NPM) provide two effective strategies for further enhancing the performance of

	NPMS. On this basis, we consider the M1.4 milestone to have been met.
Task 2: **Proof of Nanophononic Device Concept**	
M2.1 Thermal conductivity reduction in nanofabricated membrane	**Baseline End: 04/01/20 (Q4)** **% Comp 100%** Description: Demonstrate 75% thermal conductivity reduction due to nanowalls on membranes and show agreement in Modelling in Milestone 1.2. Performer Summary: Impact of COVID-19 has prevented the NIST team the necessary level of access to their facilities, which has led to the delay in demonstrating 75% reduction in the thermal conductivity. During Q6, the team made progress and reached a roughly 62% reduction, despite continued impact by COVID-19. During Q7, a new set back occurred dur to an equipment failure. The team progressed, however in further developing analysis tools and thorough design of several wafers incorporating a large number of devices. During Q8, the 75% reduction of thermal conductivity target has been met. Please see submitted Q8 report for more details.
M2.2 Test structures and measurement architecture; compare with controls	**Baseline End: 10/01/20 (Q6)** **% Comp 100%** Description: Test structure developed to measure Seebeck coefficient, electrical conductivity, and thermal conductivity for membranes with and without nanowalls, both supported on aerogel, and compare with

	control silicon membrane suspended in air. Measurement of no change in the Seebeck coefficient, no change in the electrical conductivity, and at least 85% reduction in the thermal conductivity (compared to control case of membrane with no nanowalls). Performer Summary: Impact of COVID-19 has prevented the NIST team the necessary level of access to their facilities over a period of at least six quarters leading to an accumulative delay. Despite these delays, the team has now demonstrated all aspects of this milestone using an improved test structure rather than the one originally envisioned. With this new design, we have demonstrated several test structures with thermal conductivity reduction >= 85 %, and no changes in Seebeck coefficient or electrical conductivity for membranes with and without NPM walls. In addition, we have shown that the thermal conductivity of membranes both with and without NPM walls is unaffected by encapsulation in aerogel.
M2.3 Go/No-Go: Integrated TE device proof-of-concept	**Baseline End: 04/01/21 (Q8)** **% Comp 94 %** Description: Demonstrate efficiency > 8% for at least one TE test structure at delta T = 300 K and power generated at > 0.1 W/cm2, and measure efficiency of control sample with membranes without nanowalls. Performer Summary: Impact of COVID-19 has prevented the NIST team from having the necessary level of access to their facilities over a

	period of at least six quarters leading to an accumulative delay, with approximately normal operations resuming at the end of year 3, or Q12. In Q17 we developed a process for enhancing dopant concentration near the surface and demonstrated that it lowered the contact resistance to an acceptable value. We tested the new epitaxial wafer for thermal conductivity, and while the bulk values were promising, the NPM effect was not strong. The structures had thicker membranes than our higher performing test structures, so we confirm that the NPM effect is highly sensitive to membrane thickness as indicated from theoretical work on much smaller structures.
Task 3: **Viable Device Prototype**	
M3.1 Ultra-low thermal conductivity, robust aerogel	**Baseline End: 04/01/21 (Q8)** **% Comp 100 %** Description: Optimize aerogel crosslinking chemistry for thermal conductivity below 12 mW/K-m without membrane collapse, and demonstrate compatibility with silicon components by ensuring, through electrical conductivity measurements and spot checks by microscopy, that no more that 10% of NPMs mechanically fail by membrane or nanowall breakage or nanowalls touching each other. Performer Summary: We have met all expected technical targets and performed all remaining mechanical characterizations at elevated temperatures and controlled

		mechanical properties to avoid occasional cracking of aerogel during the final assembly via improving adhesion of aerogel to copper surfaces. We resolved all issues related to compatibility of the process that resulted in oxidation in relation to integration of aerogels with metal structures, which we have refined to eliminate this problem. We have shown it being fully compatible with the aerogel drying and preparation procedures and further refined the procedures. The extensive mechanical characterization reveals that our aerogels are suitable for thermal packaging of the thermoelectric devices. Finally, we have tested and confirmed performance of aerogels when subjected to large thermal gradients (>300C difference on hot/cold sides), which is currently being performed.
M3.2 Efficient TE device demonstration	**Baseline End (extended): 10/01/22 (Q14)** **% Comp 45%**	
	Description:	Demonstrate efficiency > 18% for TE device operating at T_{hot}= 600 K, T_{cold} = 300 K (delta T = 300 K) with power generation of 0.5 W/cm2 and operating voltage of 10 mV. Report data on five replica devices with at least three meeting specification. Device area to be 0.5-1 cm^2. Report efficiency data on control devices (1) with membranes with no walls and (2) thick legs of silicon.
	Performer Summary:	We have demonstrated an unprecedented thermal conductivity reduction of over 90 % and thermal conductivities as

	low as 3.5 W/m·K, which demonstrate that our NPM materials should be able to achieve a device-level energy conversion efficiency of at least 4 %. We have identified a process for fabricating 1-cm^2 thermoelectric device layers using sapphire carrier wafers and commercial temporary wafer bond polymers. Several aspects of packaging, assembly and aerogel integration have been successfully addressed. We have received a higher quality silicon SOI wafer with a thick device layer suitable for our 1-cm^2 device design, and this material is expected to have significantly improved thermal properties over the SOI surplus wafers we have been using throughout the program. We have tested the thinner epitaxial wafer and found bulk properties to be promising. We have an improved electrical contacting scheme for the epitaxial silicon wafers. We have also developed a plan to process mechanical and electrical test die from conventional thick SOI.
Task 4: **Technology-to-Market**	
M4.1 Technoeconomic analysis to guide technology development	**Baseline End: 10/01/20 (Q6)** **% Comp 100 %** Description: Report on cost model and advanced performance model dependence on key TE device parameters including Tornado cost sensitivity analysis. Performer Summary: The team has refined the cost model and analyzed the key drivers for cost as well as the interaction of key TE device

	performance parameters. The M4.1 milestone has been fulfilled.
M4.2 Ensure technology is taken forward	**Baseline End (extended): 10/01/22 (Q14)** **% Comp 50 %** Description: Identify first market, make IP filings, and prepare presentations suitable for most promising potential funders Performer Summary: In addition to the portfolio of patents filed by the University of Colorado on the NPM concept prior to the start of this project, the university filed an additional patent application for the device concepts included in our original proposal to ARPA-E. During the program itself, we have submitted two invention disclosures covering our modified "stack" device design and our new mask layer for deep etches. Both of these disclosures were submitted as provisional patents at the end of June 2023. The university is refraining from filing patents until future publications would necessitate patent protection for these ideas, thus lengthening the period of patent applicability. We published one paper on abstract mathematical analysis of local resonances (*Journal of Sound and Vib*ration **514**, 116428, 2021). We have published a key paper in *Advanced Materials* on the first experimental results on the NPM effect and separation of thermal and electrical properties (based on data obtained prior to this grant). This paper received attention from national media (featured in IEEE Spectrum news) and led to an inquiry from

	Kyocera. We still plan to submit another paper to *Science* based on the world-record efficiency for low thermal conductivity in silicon and the new form of heat conduction that emerges from our work. PI and NIST Senior Personnel attended the ARPA-E Energy Innovation Summit and discussed future funding options with summit attendees.

Project Outputs

Journal Papers:

Bryan T. Spann, Joel C. Weber, Matt D. Brubaker, Todd E. Harvey, Lina Yang, Hossein Honarvar, Chia-Nien Tsai, Andrew C. Treglia, Minhyea Lee, Mahmoud I. Hussein, and Kris A. Bertness, Semiconductor Thermal and Electrical Properties Decoupled by Localized Phonon Resonances, *Advanced Materials* **35**, 2209779 (2023); DOI: 10.1002/adma.202209779
This article feature as a cover image in the journal.

Patents:

Two provisional patents were filed by the team, and several more are planned.

Media:

A press release was issued by NIST on May 19, 2023, titled, "NIST Team Demonstrates Novel Way to Convert Heat to Electricity"
https://www.nist.gov/news-events/news/2023/05/nist-team-demonstrates-novel-way-convert-heatelectricity

A media article was published by IEEE Spectrum on the Advanced Materials work. It was published on June 5, 2023, and titled, "Microscopic Pillars Can Recycle Waste Heat as Energy".
https://spectrum.ieee.org/thermoelectric-generator

Follow-on Funding

No follow-up funding to date. The team plans to submit a proposal in January 2025 to the NSF DMREF program.